

# The flux of electron antineutrinos from supernova SN1987A data

---

Riccardo Maria Bozza,<sup>a</sup> Vigilante di Risi,<sup>a</sup> Giuseppe Matteucci,<sup>a</sup> Veronica Oliviero,<sup>a</sup> Giulia Ricciardi,<sup>a</sup> Francesco Vissani<sup>b</sup>

<sup>a</sup>*Dipartimento di Fisica E. Pancini, Università di Napoli Federico II  
and INFN, Sezione di Napoli*

*Complesso Universitario di Monte Sant'Angelo, Via Cinthia, Napoli (NA), Italy.*

<sup>b</sup>*INFN, Laboratori Nazionali del Gran Sasso, 67100 Assergi, L'Aquila (AQ), Italy.*

*E-mail:* [riccardomaria.bozza@unina.it](mailto:riccardomaria.bozza@unina.it), [vigilante.dirisi@unina.it](mailto:vigilante.dirisi@unina.it),  
[giuseppe.matteucci@unina.it](mailto:giuseppe.matteucci@unina.it), [veronica.oliviero2@unina.it](mailto:veronica.oliviero2@unina.it),  
[giulia.ricciardi2@unina.it](mailto:giulia.ricciardi2@unina.it), [francesco.vissani@lngs.infn.it](mailto:francesco.vissani@lngs.infn.it)

**ABSTRACT:** By adopting a state-of-the-art parameterized model of electron antineutrino emission, we have made some steps forward in the analysis of the thermodynamical properties and temporal structure of neutrino emission from core collapse SN1987A. Our analysis, unlike similar previous ones, takes into account the times, energies and angles of arrival of the detected events in a reliable framework which includes a finite ramp in the initial stage of the neutrino emission. The existence of the accretion phase is confirmed with a confidence level of about 99%, and the neutrons involved in the emission during accretion, for the first time, do not show significant tensions with expectations, being about  $0.02 M_{\odot}$ . We determine the parameters of the cooling emission and discuss its duration, that compares well with theoretical expectations. We estimate the delay times between the first neutrino and the first event in the detectors. The goodness of fit checks, performed on the temporal, energy and angular distributions, show that the flux resulting from the best-fit analysis is compatible with the observed data.

**KEYWORDS:** Neutrino emission, Supernova, SN1987A, neutrino flux

---

## Contents

<b>1</b>	<b>Introduction</b>	<b>1</b>
<b>2</b>	<b>Neutrino emission in core collapse supernovae</b>	<b>2</b>
2.1	Accretion and cooling	2
2.2	Time evolution of the $\bar{\nu}_e$ emission	4
<b>3</b>	<b>Signal and detector response</b>	<b>6</b>
3.1	Inverse beta decay	6
3.2	Modeling the detector response	7
3.3	The response functions in detail	8
<b>4</b>	<b>Data analysis</b>	<b>10</b>
4.1	Methodology	10
4.2	Parameter determination	11
<b>5</b>	<b>Results</b>	<b>12</b>
5.1	Summary	13
5.2	Rising time	13
5.3	Delay times	14
5.4	Accretion emission	15
5.5	Cooling emission	15
5.6	Goodness of Fit	17
<b>6</b>	<b>Conclusions</b>	<b>20</b>
<b>7</b>	<b>Acknowledgments</b>	<b>21</b>

---

## 1 Introduction

It is generally accepted that the role played by neutrinos in core collapse supernovae (SN) is crucial, both for the energy transport and the formation of a neutron star [1–20]. In 1987, three neutrino detectors recorded a few dozen of events [21–25] which appeared simultaneous, within the limits of their time uncertainties. These were the first neutrinos that could be attributed with certainty to an extrasolar source, the supernova SN1987A. After so long, they remain the only detected supernova neutrinos. Their significance must be assessed as accurately as possible, in order to offer directions for the analysis of the much higher number of neutrinos expected from a future (nearby) supernova. A particular relevant and interesting aspect, indicated by the most detailed analyses of the SN1987A events [26, 27], is the evidence of two distinct phases of neutrino emission.

In this paper, we proceed to analyze the SN1987 neutrino events in a time window of 30s taking into account time, energy and scattering angle of the events (see table 1), with the aim of extracting the maximum information with a state-of-the-art statistical and theoretical approach. We improve on earlier reference analyses [26–29] by using a model for SN1987A neutrino emission that, in consistence with simulations, includes a finite signal rise time [30]. We perform a statistical analysis which is in many ways more refined and accurate than previous ones, and estimate the physically motivated parameters of the model together with their uncertainty intervals. In this way, we obtain new quantitative and more robust results on the temporal and energy structure of the neutrino emission, and in particular on the duration and intensity of the two main emission phases, and on the delay times between the first neutrino and the first event in the detectors. We estimate the neutrons involved in the emission during accretion, which for the first time do not exhibit significant discrepancies with expectations, being between 0.01 and 0.04  $M_{\odot}$ . Finally, we evaluate the goodness of fit of the model indicated by the analysis.

## 2 Neutrino emission in core collapse supernovae

Up to date, the only neutrino data from a core collapse supernova (SN) available are the neutrino events following SN1987A, that exploded in the Magellanic Cloud at a distance of  $D = 51.4 \pm 1.2$  kpc [31].<sup>1</sup> They were collected by Kamiokande-II, the Irvine-Michigan-Brookhaven detector (IMB) and the Baksan Neutrino Observatory (BNO) in three mutually compatible time windows [21–25].<sup>2</sup> Although SNs produce neutrinos of all flavours, these detectors were practically sensitive only to electronic antineutrinos, which are the focus of our analysis.

### 2.1 Accretion and cooling

From the beginning all the relevant simulations [1–20], based on different theoretical modeling of the SN explosion, have shown the existence of an initial and very intense neutrino emission. This harmonizes with the results of the time-energy analyses of SN1987A data [26, 29, 39, 40]: there is an initial non-thermal neutrino emission during the formation of the neutron star lasting a fraction of second (accretion), followed by a longer phase of thermal emission (cooling). We adopt a parametric framework [30] with three stages, which aims to model not only the accretion and cooling phases, but also the brief initial phase in which the brightness increases, that will be observable in future [30, 39, 41].

The choice of which model to adopt for neutrino emission is crucial for the analyses. In principle, models derived from *ab initio* calculations would be preferable. The problem, however, is that in general the numerical simulations still fail to provide an accurate estimate of uncertainty.

---

<sup>1</sup>See e.g. [20, 32, 33] for historical and didactic descriptions of SN physics.

<sup>2</sup>It would be interesting to include the two events that LSD has observed in the 30s time window which includes the neutrino burst recorded by the other detectors; however, from the existing literature [34–38], we were unable to find the information on the background, that we need to perform the analysis.

	Relative time [ms]	Energy [MeV]	SN-angle [deg]	Backgr. [Hz/MeV]		Relative time [ms]	Energy [MeV]	SN-angle [deg]	Backgr. [Hz/MeV]
K1	0	20.0±2.9	18±18	1.0E-5	I1	0	38±7	80±10	10 <sup>-5</sup> (?)
K2	107	13.5±3.2	40±27	5.4E-4	I2	412	37±7	44±15	10 <sup>-5</sup> (?)
K3	303	7.5±2.0	108±32	2.4E-2	I3	650	28±6	56±20	10 <sup>-5</sup> (?)
K4	324	9.2±2.7	70±30	2.8E-3	I4	1141	39±7	65±20	10 <sup>-5</sup> (?)
K5	507	12.8±2.9	135±23	5.3E-4	I5	1562	36±9	33±15	10 <sup>-5</sup> (?)
K6	686	6.3±1.7	68±77	7.9E-2	I6	2684	36±6	52±10	10 <sup>-5</sup> (?)
K7	1541	35.4±8.0	32±16	5.0E-6	I7	5010	19±5	42±20	10 <sup>-5</sup> (?)
K8	1728	21.0±4.2	30±18	1.0E-5	I8	5582	22±5	104±20	10 <sup>-5</sup> (?)
K9	1915	19.8±3.2	38±22	1.0E-5					
K10	9219	8.6±2.7	122±30	4.2E-3					
K11	10433	13.0±2.6	49±26	4.0E-4					
K12	12439	8.9±1.9	91±39	3.2E-3	B1	0	12.0±2.4	90(?)	8.4E-4
K13	17641	6.5±1.6	103 ± 50	7.3E-2	B2	435	17.9±3.6	90(?)	1.3E-3
K14	20257	5.4±1.4	110 ± 50	5.3E-2	B3	1710	23.5±4.7	90(?)	1.2E-3
K15	21355	4.6±1.3	120 ± 50	1.8E-2	B4	7687	17.5±3.5	90(?)	1.3E-3
K16	23814	6.5±1.6	112 ± 50	7.3E-2	B5	9099	20.3±4.1	90(?)	1.3E-3

**Table 1:** *Properties of the events in the neutrino bursts observed in the occasion of SN1987A. The events are indicated by K1, K2... K16 for Kamiokande-II [21, 22, 42]; I1, I2... I8 for IMB [23, 24]; B1, B2 ... B5 for Baksan [25]. The background in last column is taken from table 1 in [43]. A question mark reminds us that the background rate at the given energies and angles in IMB, and the directions of arrival of events in Baksan are not measured. We adopt the values in the table, since we have verified that the analysis does not depend critically on them.*

This state of affairs calls forth the adoption of models which are motivated by the physics of the problem and include parameters capable of describing theoretical uncertainties. In this way, data analysis can proceed without relying on hypotheses that are not fully consolidated or based on quantitative details at risk of subsequent reconsideration. Parametric models with well motivated parameters are also easy to interpret and adaptable to future observations.

We improve on the most common types of models used in data analysis—those that assume quasi-thermal distributions, neglect the accretion phase altogether or describe it partially. The presence of a third stage is required in order to give a smooth behavior of the observable neutrino distributions in the whole time range [30]. This amends models where the accretion phase starts at the luminosity peak, such as in refs. [26, 27, 29].

The  $\bar{\nu}_e$  spectrum, differential in time and energy, is given, in each instant of the emission, by the sum of a component of accretion (a) and one of cooling (c):

$$\frac{d\dot{N}_\nu}{dE_\nu} = \frac{d\dot{N}_{\nu,a}}{dE_\nu} + \frac{d\dot{N}_{\nu,c}}{dE_\nu}. \quad (2.1)$$

The emitted spectrum of the thermal cooling is given by [30]

$$\frac{d\dot{N}_{\nu,c}}{dE_\nu} = \frac{c}{(hc)^3} \times \pi R_{ns}^2 \times \frac{4\pi E_\nu^2}{1 + \exp(E_\nu/T_c)}, \quad (2.2)$$

where  $R_{ns}$  is the radius of the nascent proto-neutron star and  $T_c$  is its temperature.

Let us move to the discussion of emission in the accretion phase. We indicate with  $T_a$  the temperature of the positrons, and  $N_n$  the number of neutrons of the SN outer core that participate in antineutrino production via  $e^+ + n \rightarrow p + \bar{\nu}_e$ . It is convenient to express the latter as  $N_n = \xi_n \times M_\odot/m_n$ , where  $\xi_n$  quantifies the *fraction of neutron mass* contained in one solar mass of neutrons ( $M_\odot$  is the mass of the Sun,  $m_n$  the mass of one neutron). The rate of emission of electron antineutrinos in the accreting region is given by [30]:

$$\frac{d\dot{N}_{\nu,a}}{dE_\nu} = \frac{c}{(hc)^3} \times \xi_n \times \frac{M_\odot}{m_n} \times \sigma_{e+n}(E_\nu) \times \frac{8\pi E_e^2}{1 + \exp(E_e/T_a)}, \quad (2.3)$$

where  $E_e$  is the positron energy and  $\sigma_{e+n}(E_\nu)$  is the cross-section for the process of positron capture. The non-thermality of the spectrum is evident from the dependence on  $\sigma_{e+n}(E_\nu)$ . The dependence of  $E_e$  and  $\sigma_{e+n}$  on the antineutrino energy  $E_\nu$  is given in [27].

## 2.2 Time evolution of the $\bar{\nu}_e$ emission

It is convenient to assume that the luminosities of the accretion and cooling components of the spectrum each have two distinct phases: a first, common one, characterized by a rapid increase in emission, followed by a second phase, during which the emission decreases, but with different time constants  $\tau$  for accretion and cooling. The two phases are linked in a smooth manner by adopting a function of time  $\mathfrak{F}(t)$  which initially grows to  $t = t_{\max}$  – where  $\mathfrak{F}(t_{\max}) = 1$  – and then slowly decreases, namely [30]:

$$\mathfrak{F}(t, t_{\max}, \tau, \alpha) = \left( \frac{1 + \alpha \left(\frac{t_{\max}}{t}\right)^\alpha}{\exp\left[2\left(\left(\frac{t}{\tau}\right)^\alpha - \left(\frac{t_{\max}}{\tau}\right)^\alpha\right)\right] + \alpha \left(\frac{t_{\max}}{\tau}\right)^\alpha \left(\frac{t_{\max}}{t}\right)^2} \right)^{\frac{1}{2}}. \quad (2.4)$$

where the parameter  $\alpha$  governs the long-time exponential decrease of the function  $\mathfrak{F}$ :  $\alpha = 2$  for accretion and  $\alpha = 1$  for cooling. In this way, we reproduce the temporal characteristics of the emission suggested by simulations in a simple way and we can vary the parameters to account for residual theoretical uncertainties. The luminosity resulting from our analysis, displaying the various phases of electron antineutrino emission, is presented in figure 1.

For data analysis we consider the model advocated in eqs. (28) and (29) of [30], that we recall here. As the accretion phase proceeds, we can reasonably assume that the positron temperature  $T_a$  does not vary much, while the neutron density  $\xi_n$  varies in time. Furthermore, it seems safe to presume that the radius  $R_{ns}$  of the nascent neutron star stays approximately constant, while its temperature  $T_c$  varies in time as it cools down until the end of the emission. <sup>3</sup>

---

<sup>3</sup>Let us point out that alternative descriptions of the time evolution of the parameters are also possible. For example, a scenario where the neutron star radius decreases and the cooling temperature remains constant is suggested in [30], although deemed less reasonable on physical grounds.

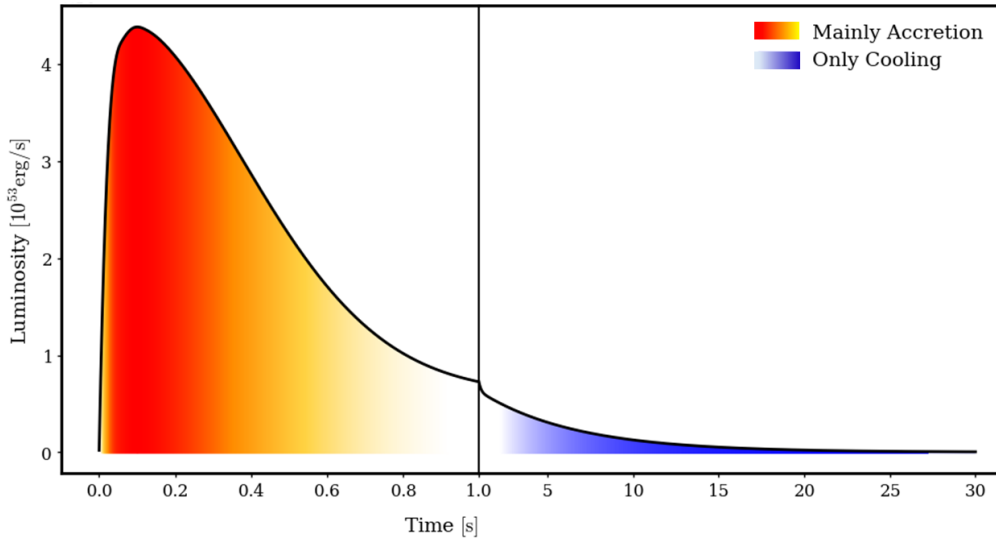


**Figure 1:** Antineutrino luminosity obtained by evaluating our model at the best fit points. The color scale is used to discriminate between the phase which is mainly accretion (red-orange) and the subsequent only cooling phase (blue). Note the different time units in the left and right panels.

The expression for the antineutrino flux is straightforwardly obtained by the emission spectra:

$$\Phi_{\bar{\nu}_e}(E_{\nu_e}, t) = \frac{1}{4\pi D^2} \left( \frac{d\dot{N}_{\nu,a}}{dE_{\nu}} + \frac{d\dot{N}_{\nu,c}}{dE_{\nu}} \right), \quad (2.5)$$

where  $D$  is the distance of the Earth from the supernova. As anticipated, its variation in time is transparently encoded in the time dependence of the parameters  $T_c$  and  $\xi_n$ , thus allowing for an efficient comparison with the experimental data. We have:

$$\begin{aligned} T_c(t) &= T_0 \times \sqrt[4]{\mathfrak{F}(t, t_{\max}, \tau_c, 1)}, \\ \xi_n(t) &= \xi_{n0} \times \mathfrak{F}(t, t_{\max}, \tau_a, 2), \end{aligned} \quad (2.6)$$

where  $T_0$  is the temperature related to the average energy of antineutrinos, the number of neutrons,  $\xi_{n0}$ , parameterizes the intensities of the accretion emission and the fourth root accounts for the fact that the luminosity (proportional to  $T_c^4$ ) scales with the function  $\mathfrak{F}$ .  $T_0$  and  $\xi_{n0}$  are also the values at the maximum of the initial ramp, that is when  $t = t_{\max}$ . The time parameters  $\tau_a$  and  $\tau_c$  characterize the accretion and the cooling phases, respectively. We also set:

$$R_{ns}(t) = R_{ns0}, \quad (2.7)$$

$$T_a(t) = 0.6 \times T_0. \quad (2.8)$$

The second condition is determined by smoothly matching the average energies of the antineutrinos in the two phases of the emission.

A much debated point is the role of neutrino oscillations in supernovae. Some aspects have been investigated, like the role of the matter effect [44, 45] and the non-linear nature of the process [46], but the overall discussion of this plausible possibility does not seem to have reached a conclusion yet [47]. The application of these theoretical representations to neutrino emission from SN1987A has also occasioned an intense discussion. Several older analyses have suggested that oscillations play an important role [48–50], while more recent studies, beginning with [51, 52], have pointed out that astrophysical uncertainties hinder the ability to draw firm conclusion. An interesting insight emerged by quantitative analyses of the SN1987A data [27, 40], recently reaffirmed [29], namely that the oscillations do not play an important role in the case of a ‘normal’ mass spectrum, while in the case of a ‘inverse’ mass spectrum there is a potentially interesting effect during the accretion phase. However, the latter conclusion is subject to a number of uncertainties, due to the incomplete modeling of the oscillations and the neutrino emission itself. In any case, theoretical expectations, as well as experimental results, seem to point towards the ‘normal’ mass spectrum case [53–55].

In light of these considerations, we feel justified in assuming normal mass ordering and we do not add effects due to neutrino oscillations. To be even more conservative and precise, we can say that the neutrino flux we obtain from our analysis of SN1987A data is to be considered as an effective flux, already including the effects of neutrino oscillations. Its precise meaning in relation to astrophysics requires progress that is currently unavailable, but which we expect would not change the conclusions by more than a dozen percentage points.

### 3 Signal and detector response

#### 3.1 Inverse beta decay

The inverse beta decay (IBD)

$$\bar{\nu}_e + p \rightarrow n + e^+ \quad (3.1)$$

is by far the most relevant channel for non-thermal processes and the hypotheses that the SN1987A signal in the accretion region is entirely due to IBD is quite reliable [43, 56–59].

<sup>4</sup> We use all the available data on energy, time and the angle  $\theta$  between the antineutrino and the positron provided by Kamiokande-II [21, 22], IMB [23, 24] and Baksan [25] and reported in table 1.

For an ideal detector, the IBD positron spectrum, triply differential in time  $t$ , positron energy  $E_e$ , and  $\cos\theta$ , is given by

$$S_e(E_e, \cos\theta, t) = N_p \times \Phi_{\bar{\nu}_e}(E_\nu, t) \times \frac{d\sigma^{\text{IBD}}}{dE_e}(E_\nu, E_e) \times J(E_\nu, \cos\theta), \quad (3.2)$$

where  $N_p$  is the number of protons of the detector and  $J(E_\nu, \cos\theta)$  is the Jacobian of the differential flux. For the IBD cross section  $d\sigma^{\text{IBD}}$  we adopt the most recent and accurate calculation to date [60].

---

<sup>4</sup>The possibility of other types of events besides IBD is discussed in several works, starting with [56]; however, this is considered less plausible by recent quantitative discussions, such as [43].

Detector	$M_{\text{det}} [10^9 \text{ g}]$	Molecule	$n$	$m_{\text{mol}} [10^{-23} \text{ g}]$	$N_p [10^{32}]$
Kam-II	2.14	H <sub>2</sub> O	2	2.9915	1.430
IMB	6.8	H <sub>2</sub> O	2	2.9915	4.546
Baksan	0.2	C <sub>9</sub> H <sub>20</sub>	20	21.297	0.188

**Table 2:** Mass, molecular composition, stoichiometric number of hydrogen, molecular mass and number of free protons for each detector. The information on masses and composition of the detectors are taken from literature [21, 25, 61]

The number of free protons  $N_p$  (hydrogen atoms) in each detector is calculated by means of the formula

$$N_p = n(1 - Y_D) \frac{M_{\text{det}}}{m_{\text{mol}}} \quad (3.3)$$

where  $n$  is the stoichiometric number of hydrogen in the molecules which constitute the detectors,  $Y_D = 0.0145\%$  is the deuterium abundance (as on Earth, in oceans it is slightly more),  $M_{\text{det}}$  is the mass of the detectors (1kton =  $10^9$  g) and  $m_{\text{mol}}$  is the mass of the molecules that compose the detectors. Values and results are reported in table 2.

### 3.2 Modeling the detector response

The relation between  $S_e$  and the signal  $S$ , the spectra actually observed by the detectors, can be described as a convolution of  $S_e$  with the intrinsic efficiency function  $\eta(E_e)$  and an ad-hoc Gaussian smearing function  $G(E_e - E_i, \sigma(E_e))$ , where  $E_i$  is the measured value of the positron energy and  $\sigma(E_e)$  the standard deviation:

$$S(E_i, \cos \theta, t) = \int_{m_e}^{\infty} \zeta(\cos \theta) \eta(E_e) G(E_e - E_i, \sigma(E_e)) S_e(E_e, \cos \theta, t) dE_e. \quad (3.4)$$

Here  $m_e$  is the positron mass and the function  $\zeta(\cos \theta)$  is the angular bias function of the detector, which is provided by the experimental collaboration [21–25]. The total efficiency of the detector is also supplied, but not the efficiency function  $\eta(E_e)$ . We recover the unknown  $\eta(E_e)$  and  $\sigma(E_e)$  by extrapolation, as described in section 3.3. We have tested minor variations in the function parametrizations and verified that they do not critically affect the global fits or alter the key conclusions regarding the SN1987A neutrino signal.

The advantage of eq. (3.4) is that, by setting an appropriate minimal value  $E_{\text{min}}$  on the observed positron energy, one can take into account the entire SN1987A dataset and background *a posteriori* rather than *a priori*. Moreover, the number of total events  $N_{\text{tot}}$  can be estimated by integrating the observed signal and background over a wide time window (0 to 30 s), avoiding biases, over the entire range for  $\cos \theta$  (-1 to 1) and above the threshold  $E_{\text{min}}$  for the positron energy:

$$N_{\text{tot}}(E_{\text{min}}) = N_{\text{bkg}} + \int_{E_{\text{min}}}^{\infty} \zeta(\cos \theta) \varepsilon(E_e, E_{\text{min}}) S_e(E_e, \cos \theta, t) dE_e d\cos \theta dt. \quad (3.5)$$

The information on the total number of events due to background  $N_{\text{bkg}}$  is taken from table 2 in ref. [43]. The function  $\varepsilon(E_e, E_{\text{min}})$  is the total efficiency of the detectors, which results



by integrating the Gaussian smearing function:

$$\varepsilon(E_e, E_{\min}) = \eta(E_e) \times \frac{1 + \operatorname{erf}\left(\frac{E_e - E_{\min}}{\sqrt{2}\sigma(E_e)}\right)}{2}, \quad (3.6)$$

where erf is the Gauss error function. The values for  $E_{\min}$  used in the analysis are listed in table 3 and discussed in section 3.3. We recover the total efficiency and number of events provided by the experimental collaborations [21–25]. Our procedure is in agreement with that outlined in [62], and it is also adopted in more recent analyses, such as [43] and [29]. Instead, some of the most careful analyses of the SN1987A data so far, namely [26, 27], adopt a suboptimal procedure for the inclusion of efficiency, which introduces a bias in the interpretation of their results, as discussed in [43].

### 3.3 The response functions in detail

In this section, we provide more details on how we model the response of the three detectors considered. Our approach refines a procedure already adopted e.g. in refs. [43, 62]. Eq. (3.4) describes a linear functional which correlates the observed and true energy. For each detector, three ingredients are needed to build this functional:

- the energy resolution  $\sigma(E_e)$ , which describes the spread between the true positron energy  $E_e$  and the reconstructed energy  $E_i$ ;
- the intrinsic efficiency  $\eta(E_e)$ , which characterizes the efficiency of the detector and the reconstruction process, factoring out resolution effects;
- the angular bias  $\zeta(\cos\theta)$ , which is needed to take directional inefficiencies into account.

**Energy resolution  $\sigma(E_e)$ :** Each experiment measures the energy of the emitted positron with finite resolution, modeled by a Gaussian kernel:

$$G(E_e - E_i, \sigma(E_e)) = \frac{1}{\sqrt{2\pi}\sigma(E_e)} \exp\left[-\frac{(E_e - E_i)^2}{2\sigma(E_e)^2}\right]. \quad (3.7)$$

We parametrize the energy resolution as

$$\sigma(E_e) = \sigma_{\text{stat}} \sqrt{\frac{E_e}{10 \text{ MeV}}} + \sigma_{\text{syst}} \frac{E_e}{10 \text{ MeV}}, \quad (3.8)$$

where  $\sigma_{\text{stat}}$  and  $\sigma_{\text{syst}}$  are constants fitted to the energy uncertainties of each detector reported in table 1.

In figure 2 we show the best fit  $\sigma(E_e)$  curves (solid lines) superimposed on the points provided by Kamiokande-II, IMB and Baksan. The corresponding resolution functions for each experiment are collected in table 3.

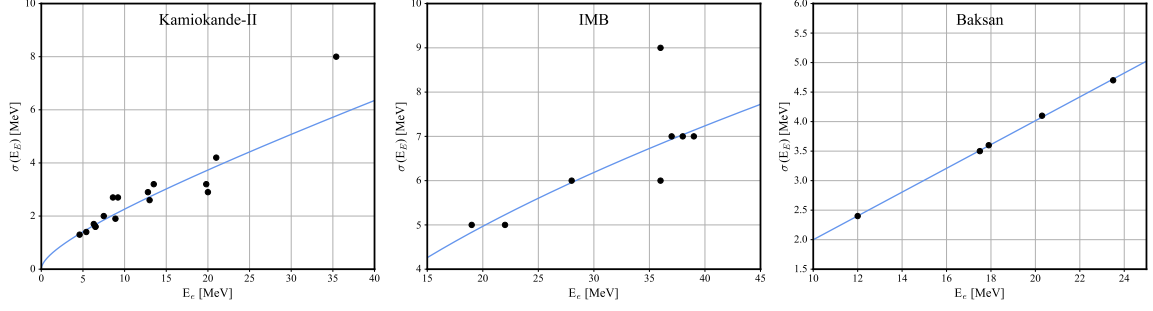


**Figure 2:** Parametrization of the uncertainty  $\sigma(E_e)$  for each detector (Kamiokande-II, IMB, and Baksan) as a function of the positron energy  $E_e$ .

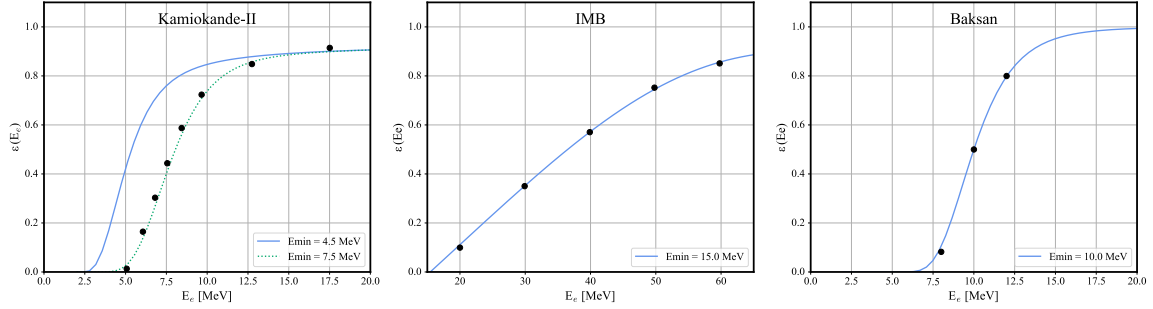


**Figure 3:** Detection efficiency  $\varepsilon(E_e)$  as a function of electron energy  $E_e$  for the three detectors: Kamiokande-II, IMB, and Baksan. The parametrization of the efficiency curves is based on detector-specific acceptance thresholds,  $E_{\min}$ , as indicated in the legend. Black points represent the reported efficiency values from the detectors. The continuous lines show the efficiency curves that we use for the analysis.

**Intrinsic and total efficiency:** The total probability that a positron of true energy  $E_e$  is recorded as an event includes two key factors. The first is the threshold cut  $E_{\min}$ , which is the minimum energy to admit an event in the analysis. We adopt  $E_{\min} = 4.5$  MeV for Kamiokande-II in agreement with [43]. We use all the events observed from SN1987A in the analysis, rather than excluding some by attributing them *a priori* to background processes; in particular, we also consider K13, K14, K15, and K16 and the events recorded by Baksan. The second factor is the intrinsic efficiency  $\eta(E_e)$ , which represents the fraction of events passing trigger, reconstruction, and identification, excluding resolution effects. While  $\eta(E_e)$  can be set to 1 in scintillators such as Baksan due to their high light yield, this is not the case for Cherenkov detectors.

To capture these effects together, we write the detector efficiency as in eq. (3.6). We have adopted the parametrization and values for  $\eta(E_e)$  provided by ref. [43].<sup>5</sup> Figure 3 shows the resulting  $\varepsilon(E_e)$  curves for Kamiokande-II, IMB, and Baksan, with black markers indicating the efficiencies reported by the respective collaborations at selected energies. For

<sup>5</sup>We corrected a typo in [43] concerning the parameterisation of  $\eta$  for the IMB (eq. 14 there) and obtained slightly different coefficients, which however agree within the uncertainties.

	$E_{\min}$ [MeV]	$\eta(E_e)$	$\sigma(E_e)$ [MeV]
Kamiokande-II	4.5	$0.93 \left[ 1 - \left( \frac{0.2 \text{ MeV}}{E_e} \right) - \left( \frac{2.5 \text{ MeV}}{E_e} \right)^2 \right]$	$1.27 \left( \frac{E_e}{10 \text{ MeV}} \right)^{1/2} + 1.0 \left( \frac{E_e}{10 \text{ MeV}} \right)$
IMB	15	$0.379 \left( \frac{E_e}{15 \text{ MeV}} - 1 \right) - 6 \times 10^{-3} \left( \frac{E_e}{15 \text{ MeV}} - 1 \right)^4 + 10^{-3} \left( \frac{E_e}{15 \text{ MeV}} - 1 \right)^5$	$3.3 \left( \frac{E_e}{10 \text{ MeV}} \right)^{1/2} + 0.2 \left( \frac{E_e}{10 \text{ MeV}} \right)$
Baksan	10	1.0	$2.0 \left( \frac{E_e}{10 \text{ MeV}} \right)$

**Table 3:** Energy thresholds  $E_{\min}$ , intrinsic efficiencies  $\eta(E_e)$  and energy standard deviation functions  $\sigma(E_e)$  for Kamiokande-II, IMB and Baksan.

the reader’s convenience, the full functions are provided in table 3.

**Angular Bias:** Only for the case of IMB, the angular bias function is not trivial. At the time of SN1987A, IMB experienced a malfunctioning which affected 25% of its readout channels, biasing the directional reconstruction. In our analysis, this is taken into account with a linear correction in efficiency  $\zeta(\cos\theta) = 1 + 0.1 \cos\theta$ , following the prescription of the IMB collaboration [63].

## 4 Data analysis

### 4.1 Methodology

There are two primary and distinct types of statistical analysis which are relevant for the neutrino emission of SN1987A. One aims to identify, within a given class of parameterized models, which ones provide the best representation of the data (in particular, the best-fitting parameters with their confidence regions). The other one aspire to assess how well the observed data correspond to the fitted, assumed model, by means of goodness of fit (GOF) tests. We have performed both analyses:

- 1 the best-fit parameters of our model are obtained by minimizing the  $\chi^2$ -function, as detailed in section 4.2. In the statistical analysis, it is possible to apply a marginalization procedure by integrating over the parameters [26] or, alternatively, minimizing the  $\chi^2$ .<sup>6</sup> Although the former approach is preferable in principle, being theoretically more rigorous, it is significantly more demanding computationally. Moreover, no substantial discrepancy between the results given by the two methods is expected for the case of SN1987A [27]. We have therefore decided to adopt the latter procedure.
- 2 The GOF tests are quite standard and are detailed in section 5.6.

---

<sup>6</sup>This is equivalent to perform the maximization of the likelihood function [27] (profile likelihood).

We have chosen to perform all analyses in parallel using two different implementations and programming languages, Python and Mathematica. This decision enabled us to cross-check the results and optimize numerical computations by leveraging the combined strengths of both languages. Mathematica excels in symbolic computation and provides an extensive library of built-in functions that facilitate rapid prototyping and analytical derivations. Python, on the other hand, offers robust libraries for numerical analysis, data handling, and visualization, alongside excellent scalability and integration capabilities. By combining these strengths, we ensured that the codes developed in the two environments yield results that are highly consistent and comparable with remarkable precision.

Preliminary studies and results have already been presented [64, 65].

## 4.2 Parameter determination

The parameters of the model are estimated by minimizing the  $\chi^2$ -function

$$\chi^2 = -2 \sum_{d=k,i,b} \log \mathcal{L}_d, \quad (4.1)$$

where  $\mathcal{L}_d$  is the unbinned poissonian likelihood of any detector ( $k, i, b$  stand for Kamiokande-II, IMB and Baksan, respectively), defined as:

$$\mathcal{L}_d = e^{-f_{\text{live}} N_{\text{tot}}} \times \prod_j^{N_d} e^{S(t_d + \delta t_j + \tau_d/2) \tau_d} \times \left[ \frac{B_j}{2} + S(E_j, \cos \theta_j, t_d + \delta t_j) \right], \quad (4.2)$$

where  $S$  is the signal rate, described above, and  $B_j$  is the background given in table 1. The index  $j$  runs over the events detected by each experiment. In our emission model  $t = 0$  is the time of the arrival of the first *antineutrino* on Earth. In the likelihood, we use the time  $t_j$  of the detected event  $j$ , which can be written as

$$t_j = t_d + \delta t_j \text{ for } d = k, i, b. \quad (4.3)$$

Here  $\delta t_j$  is the (measured) time difference between each detected event and the first detected one. The parameters  $t_d$  represent the delay times between the *arrival* of the first  $\bar{\nu}_e$  on Earth ( $t = 0$ ) and the *detection* of the first event in each experiment. The delay times, first introduced in [28], are estimated from the global fit. The energies  $E_j$ , the scattering angles  $\theta_j$  and the  $\delta t_j$  of each event are collected in table 1. For IMB, we set  $\tau_d = 0.035$  s and  $f_{\text{live}} = 0.9055$  to take into account the dead-time and the muon contamination, while for both Kamiokande-II and Baksan  $\tau_d = 0$  and  $f_{\text{live}} = 1$  [26].

In addition to the delay times, the model depends on a set of 6 astrophysical parameters, identified and discussed in section 2. These are the time scales of the emission,  $t_{\text{max}}$ ,  $\tau_a$  and  $\tau_c$ , plus  $R_{ns}$ ,  $\xi_{n0}$  and  $T_0$ . We let them vary in wide ranges (our priors):

$$\begin{aligned} 1 \text{ km} \leq R_{ns} \leq 100 \text{ km} & & 0 \leq \xi_{n0} \leq 40\% & & 2 \text{ MeV} \leq T_0 \leq 6 \text{ MeV} \\ 1 \text{ s} \leq \tau_c \leq 10 \text{ s} & & 100 \text{ ms} \leq \tau_a \leq 1 \text{ s} & & 10 \text{ ms} \leq t_{\text{max}} \leq 200 \text{ ms} \\ 0 \leq t_k \leq 0.5 \text{ s} & & 0 \leq t_i \leq 0.5 \text{ s} & & 0 \leq t_b \leq 0.5 \text{ s} \end{aligned} \quad (4.4)$$

	$R_{ns0}$	$\xi_{n0}$	$T_0$	$\tau_a$	$\tau_c$	$t_k$	$t_i$	$t_b$
$R_{ns0}$	1	0.60	-0.82	-0.059	-0.15	-0.0087	0.030	0.0054
$\xi_{n0}$	0.60	1	-0.81	-0.26	0.30	-0.033	0.0097	0.0018
$T_0$	-0.82	-0.81	1	-0.0094	-0.28	0.017	-0.013	-0.0026
$\tau_a$	-0.059	-0.26	-0.0094	1	0.071	0.015	-0.066	-0.022
$\tau_c$	-0.15	0.30	-0.28	0.071	1	-0.0072	-0.013	0.00064
$t_k$	-0.087	-0.033	0.017	0.015	-0.0072	1	-0.00013	-0.000016
$t_i$	0.030	0.0097	-0.013	-0.066	-0.013	-0.00013	1	0.0019
$t_b$	0.054	0.0018	-0.0026	-0.022	0.00064	-0.000016	0.0019	1

**Table 4:** Correlation matrix of the parameters of the model when the rising time is fixed at  $t_{max} = 100$  ms. The correlation coefficients are evaluated under the hypothesis of gaussian distributed parameters.

In the following these ranges will be discussed from a physical standpoint, compared with expected values in literature, and refined in the course of the analysis. Let us emphasize that  $t_{max}$  is the time at which the antineutrino flux reaches its maximum value. Also, the time-dependent functions  $\xi_n$  and  $T_c$  are respectively proportional to  $\xi_{n0}$  and  $T_0$ .

We have estimated the confidence intervals by scanning the  $\chi^2$ -function around its minimum<sup>7</sup>, as described e.g. in [66]. Choosing a model parameter  $p$  and letting the other model parameters vary in their prior interval, first we compute the profile function  $\chi^2(p)$  from the eq. (4.1), minimizing on the remaining variables; then we subtract the value in the minimum  $p_{best}$ , and in this way we obtain  $\Delta\chi^2(p) = \chi^2(p) - \chi^2(p_{best})$ . The best fit point of the parameters (corresponding to the maximum of the likelihood function in eq. (4.2)), is now defined by the condition  $\Delta\chi^2(p) = 0$ , while the confidence level intervals are obtained by setting  $\Delta\chi^2 = 1, 6, 9$ , corresponding to  $1\sigma$ ,  $2\sigma$  and  $3\sigma$ , respectively.

## 5 Results

We start this section by summarizing the results of our analysis (best fit parameters and their uncertainties), which we discuss in detail later on. Let us preliminarily observe that we are not able to constrain simultaneously the rising time and the delay times. This can be attributed to the limited statistics from SN1987A, which does not allow to resolve appropriately the rising region. As a result we fix the parameter  $t_{max} = 100$  ms, as discussed in subsection 5.2.

<sup>7</sup>This method allows to estimate the uncertainties when the parameters are (approximatively) Gaussian distributed around their best fit value. However, even when the parameters are distributed in a non-Gaussian way it provides often a reasonable approximation for the uncertainties.

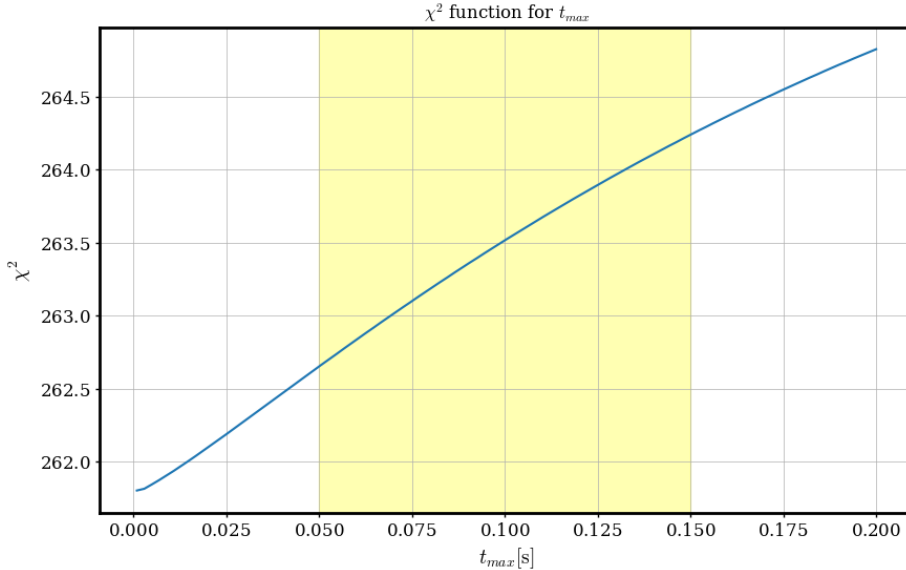


**Figure 4:** One-dimensional  $\chi^2$ -function of  $t_{\max}$ . The yellow band indicates the region preferred by the simulations and adopted in the analysis.

## 5.1 Summary

The minimum of the  $\chi^2$ -function in eq. (4.1) is found at

$$\begin{aligned}
 R_{\text{ns}0} &= (17.0)_{-0.5}^{+0.7} \text{ km}, & \xi_{n0} &= (0.018)_{-0.011}^{+0.025}, & T_0 &= (4.6)_{-0.4}^{+0.5} \text{ MeV}, \\
 t_{\max} &= 0.1 \text{ s}, & \tau_a &= (0.52)_{-0.15}^{+0.24} \text{ s}, & \tau_c &= (5.6)_{-1.3}^{+1.8} \text{ s}, \\
 t_k &= (0.035)_{-0.024}^{+0.065} \text{ s}, & t_i &= (0.043)_{-0.029}^{+0.102} \text{ s}, & t_b &= (0.054)_{-0.041}^{+0.152} \text{ s},
 \end{aligned} \tag{5.1}$$

where  $\chi^2 = 263.5$ . Further information on the best-fit points and confidence intervals can be read from the profile log-likelihood ( $\Delta\chi^2$ ) functions.

The correlation matrix computed as the second derivatives of the  $\chi^2$ -function by means of the finite difference method is displayed in table 4. Let us observe that the astrophysical parameters and the delay times are not correlated; the largest correlations concern the first three parameters. One can therefore expect the timing determinations of the two emission phases to be little affected by the rest and therefore quite reliable.

Figure 1 clearly shows the smooth connection between the two phases of accretion and cooling.

## 5.2 Rising time

Our model is characterized by an initial phase of antineutrino emission in which the luminosity increases reaching its peak at  $t = t_{\max}$  [30]. Simulations show that the expected  $t_{\max}$  is in the hundred milliseconds range [39, 41, 67, 68]. Let us investigate what insight the data from SN1987A provide. By letting  $t_{\max}$  vary in the interval  $[0.01 - 0.2]$  s, we minimize the function  $\chi^2$ . In figure 4 it is shown that the resulting  $\chi^2$  profile varies by only a few units over the interval—the data do not indicate a preferred value for  $t_{\max}$ . Therefore, in the

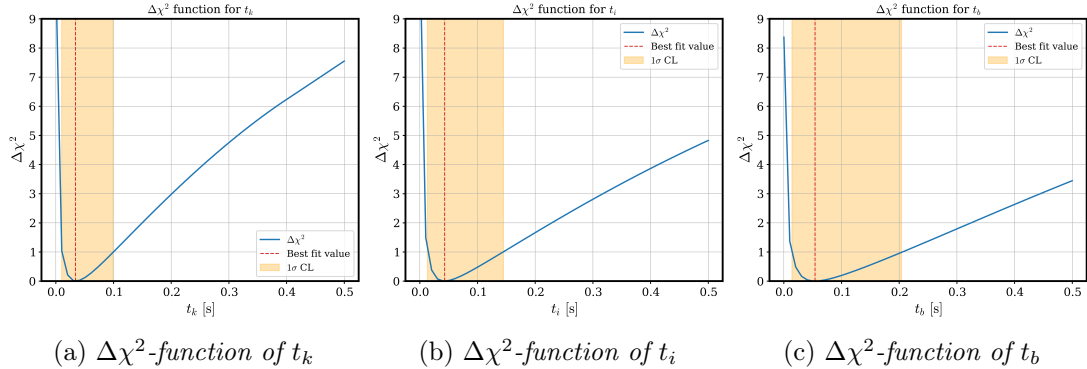


**Figure 5:**  $\Delta\chi^2$ -functions for the parameters  $t_k$ ,  $t_i$  and  $t_b$  ( $k, i, b$  stand for Kamiokande-II, IMB and Baksan, respectively). The red dashed line indicates the best fit values. The orange bands show the confidence interval at  $1\sigma$ .

following analysis we set  $t_{\max}$  at the central value  $t_{\max} = 100\text{ms}$ . The alternative procedure of letting  $t_{\max} = 0$ , which would formally correspond to the assumptions of [26, 27, 29], is not supported by the simulations.

### 5.3 Delay times

Our analysis gives the elapsed time between the arrival of the first electron antineutrino and the detection of the first signal (delay time) for each experiment, as defined in section 4.2. They are different for the three experiments, not only because of the intrinsic detection properties but also because of the different spatial locations of the experiments. The latter contribution is *a priori* shorter than the time it takes for light to cross the Earth’s diameter ( $\lesssim 2R_E/c = 43\text{ms}$ ) and in the present case, it was several times smaller and therefore practically negligible.<sup>8</sup> Looking at the temporal distribution of the very first events, we established a reasonable prior  $[0 - 0.5]$  s.

The best fit points with the uncertainties corresponding to the  $1\sigma$ -confidence intervals are:

$$t_k = (0.035)_{-0.024}^{+0.065} \text{ s}, \quad t_i = (0.043)_{-0.029}^{+0.102} \text{ s}, \quad t_b = (0.054)_{-0.041}^{+0.152} \text{ s}. \quad (5.2)$$

The orange bands in figure 5 represent the  $1\sigma$ -confidence intervals. The adoption of a model of emission with a finite, initial, rising time for the neutrino luminosity represents an improvement for the estimates of the delay times in previous analyses where the luminosity features a nonphysical discontinuity at the onset time  $t = 0$  s [26, 27, 29]. Such safe description of luminosity together with an estimation of the delay times was also performed in [28], and, as far as we can compare, the results do not disagree. However, they consider the astrophysical model fixed, do not take background into account and some events are excluded *a priori* from the analysis. Differently, we prefer to include all the events registered

<sup>8</sup>SN1987A was in the deep southern sky and the detectors were all in the northern hemisphere instead. The neutrinos reached first Kamiokande-II, then IMB and finally Baksan, after 7 and 10 ms respectively.

in the 30 s after the burst, thus using all the information provided by Kamiokande-II, IMB and Baksan.

#### 5.4 Accretion emission

The antineutrino emission in the accretion phase depends on  $\xi_{n0}$ ,  $T_0$  and  $\tau_a$ . From the procedure of minimization of the  $\chi^2$ -function we obtain best-fit values

$$\xi_{n0} = (0.018)_{-0.011}^{+0.025} \quad T_0 = (4.6)_{-0.4}^{+0.5} \text{ MeV} \quad \tau_a = (0.52)_{-0.15}^{+0.24} \text{ s.} \quad (5.3)$$

The  $\Delta\chi^2$ -functions for  $\xi_{n0}$ ,  $\tau_a$  and  $T_0$  with  $1\sigma$ -confidence intervals (orange bands) are displayed in figure 6. The accretion time  $\tau_a = 0.52$  s is perfectly compatible with an initial accretion phase of a fraction of a second. We confirm also the un-physical feature for  $\tau_a < 0.3$  s, pointed out and discussed in section 3.3 of [27].

An interesting point to consider is the statistical significance of this model compared to an emission model with only the cooling phase, which can be formally obtained by setting  $\xi_{n0} = 0$ . The variation of the minimum  $\chi^2$  between the two models is  $\Delta\chi^2 \simeq 8.2$ , a result which is somewhat weaker, but in substantial agreement with [27], where  $\Delta\chi^2 = 9.8 - 14.7$  for their models of emission.

Our result corresponds to a significance of 99.8% of the accretion hypothesis, evaluated by means of the likelihood ratio test [66, 69] and considering that the model with no accretion (null hypothesis) has one parameter fixed ( $\xi_{n0} = 0$ ). Alternatively, it could be assumed that the model without accretion actually has two fewer parameters ( $\xi_{n0}$  and  $\tau_a$ ), eventually obtaining a confidence level for the accretion of 99.2%.<sup>9</sup>

The fraction of neutrons involved in the emission,  $\xi_{n0} = 1.8\%$ , despite its large uncertainty, suggests a scenario which is quite intriguing on physical grounds: during accretion,  $\bar{\nu}_e$  are produced mainly by a thin neutron atmosphere around the nascent proto-neutron star. This result represents a significant improvement with respect to previous analyses, where a large portion of the total mass of the outer core ( $0.2 - 0.8M_\odot$ ) was instead found to be needed at best fit point to take into account the observed spectrum of SN1987A [26, 27].

#### 5.5 Cooling emission

During the cooling phase, following the explosion, there is no longer significant accretion emission and the hot neutron star settles down by emitting neutrinos. Let us point-out that the neutron star has long been sought without success, and this has caused a tension with theoretical expectations [70]. However, in 2015, very accurate simulations have showed that the hot neutron star is enveloped in a dense region of expanding gaseous remnants [71]. In addition to the indirect observational evidence collected in the last years, direct evidence has recently been obtained [72].

---

<sup>9</sup>The model with no accretion is obtained by putting  $\xi_{n0} = 0$ , which is a borderline value for the model with accretion. Consequently, the likelihood ratio  $\Delta\chi^2$  is expected to be distributed as  $f(x) = \frac{1}{2}\chi_m^2(x) + \frac{1}{2}\delta(0)$ , using the notation adopted in [69] where  $m$  represents the difference between the number of degrees of freedom within the two models. The p-value of the hypothesis with no accretion (null hypothesis) is  $\int f(x)dx$  for  $x > \Delta\chi^2$ .



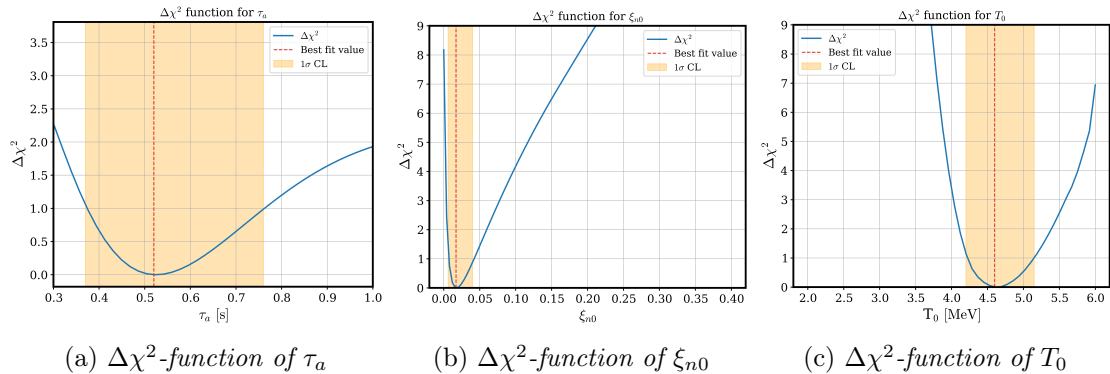


**Figure 6:**  $\Delta\chi^2$ -functions for  $\tau_a$ ,  $\xi_{n0}$  and  $T_0$ . The red dashed lines indicate the best fit value of the parameters. The orange bands show the confidence interval at  $1\sigma$ .

In our model, the cooling temperature  $T_c$  decreases over time according to eq. (2.6), while the radius  $R_{ns}$  of the neutron star remains constant. The spectrum of the emitted electronic antineutrinos is given in eq. (2.2). The parameters involved are the same temperature parameter  $T_0$  that describes the accretion emission,  $R_{ns}$ , and  $\tau_c$ .

The  $\Delta\chi^2$ -functions for  $R_{ns}$  and  $\tau_c$ , together with the  $1\sigma$ -confidence intervals (orange bands), are shown in figure 7. The numerical values for the radius and the cooling time at the best fit points are:

$$R_{ns} = (17.0)_{-0.5}^{+0.7} \text{ km}, \quad \tau_c = (5.6)_{-1.3}^{+1.8} \text{ s}. \quad (5.4)$$

The best fit value  $R_{ns} = 17\text{km}$  agrees with the expectation on the neutron star radius, improving the results of previous analyses [26, 27]—further progress will come from its direct measurement. The value for the cooling time  $\tau_c = 5.6\text{s}$  also fits well with the expected scenario of a long-standing thermal emission after the accretion [26, 27].

Recently, improved simulations of the duration of the emission have been obtained, suggesting that 95% of Kamiokande-II and IMB signal events are collected in 5 – 7 s, with some models accounting for durations up to 10 s [73]. Similarly, these simulations show that Baksan collects 95% of data in 4 – 10 s, but, differently from the analyses for Kamiokande-II and IMB, the background is included.

At the best fit point the number of events expected as signal in our model (no background) are

$$N_{\text{KII}} = 16.2 \pm 3.7 \quad N_{\text{IMB}} = 6.2 \pm 1.9 \quad N_{\text{BNO}} = 2.1 \pm 0.4, \quad (5.5)$$

The corresponding time windows to cumulate the 95% of the whole set of events are

$$\text{Kamiokande-II} \quad 10.8 \text{ s} \quad (5.6)$$

$$\text{IMB} \quad 7.3 \text{ s} \quad (5.7)$$

$$\text{BNO} \quad 9.8 \text{ s}, \quad (5.8)$$

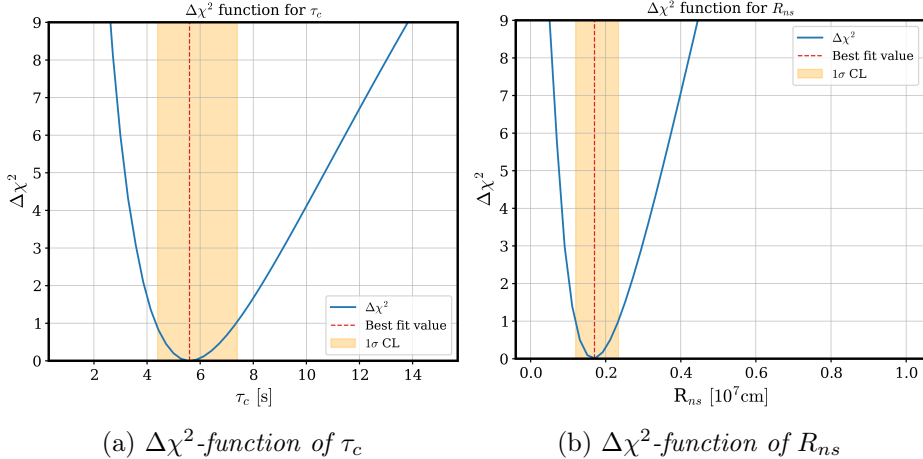


**Figure 7:**  $\Delta\chi^2$ -functions for  $\tau_c$  (left) and  $R_{ns}$  (right). The red dashed lines indicate the best fit values. The orange bands show the confidence interval at  $1\sigma$ .

in perfect agreement with some models of emission considered in ref. [73], in particular the ones with the neutron star mass of  $1.62M_\odot$  and equations of state of the stellar medium without convection. Furthermore, when uncertainties in astrophysical parameters are taken into account, our results do not contradict most of the models in tables VII and VIII of ref. [73].

## 5.6 Goodness of Fit

While obtaining the best fit parameters is an essential step of an accurate statistical analysis, it is equally important to confirm that the model reliably reproduces the observed data from SN1987A. Noteworthy in passing is that such scrutiny should apply not only to data analyses as the present one, but also to theoretical simulations of the neutrino flux emitted by SN1987A.

To ensure that our model is consistent with the observed data, we have verified its goodness of fit (GOF). We have chosen the Cramér–von Mises and Kolmogorov–Smirnov tests, which compare the empirical cumulative distribution function (ECDF) of a sample with the cumulative distribution function (CDF) of a specified theoretical distribution. The goal of the tests is to evaluate at which confidence level the data are consistent with the theoretical model.

From the observed signal, differential in energy, time and  $\cos\theta$  in eq. (3.4), and the background (see table 2 in [43]), we compute the theoretical energy, temporal and angular CDF for Kamiokande-II, Baksan, and IMB. The benchmark values for the parameters in the signal are the results of our best fit calculations. The ECDF are built with the data reported in table 1. For the comparison with the theoretical angular distribution of Kamiokande-II we perform two analyses:

- 1 we exclude the events K13, K14, K15, K16, which are usually assumed to be back-

p-values Cramér–von Mises test	Baksan	IMB	Kamiokande-II (including all events)	Kamiokande-II (excluding K13- K14-K15-K16)
Rate	77.8 %	89.4%	60.9 %	-
Energy	55.0 %	10.9 %	18.3 %	-
Angle	N/A	5.9%	38.0 %	7.0 %

p-values Kolmogorov- Smirnov test	Baksan	IMB	Kamiokande-II (including all events)	Kamiokande-II (excluding K13- K14-K15-K16)
Rate	77.9 %	91.1 %	45.6 %	-
Energy	57.3 %	4.4 %	15.9 %	-
Angle	N/A	11.9%	49.0 %	11.9 %

**Table 5:** *p-values from the comparison of the theoretical time, energy and angle cumulative distributions (CDF) with the empirical cumulative distributions (ECDF) observed by Kamiokande-II, Baksan and IMB. The p-values are computed using the Cramér–von Mises and the Kolmogorov-Smirnov tests. Baksan does not measure the direction of the events, so there is no information on the empirical angular distribution.*

ground. Consistently with this assumption we change the threshold  $E_{\min}$  to 7.5 MeV;

- 2 we include all events, hence also the events K13, K14, K15, K16, exploiting the information on the scattering angles in ref. [42].

The confidence level resulting from these tests, expressed by the p-values, are reported in table 5.

The values indicated in table 5 show that the flux obtained from our statistical analysis describes the data well, and this is particularly true for its temporal distribution. However, we note some tension between: 1) the energy spectra of Kamiokande-II (‘cooler’) and IMB (‘hotter’); 2) the angular distribution expected from the inverse beta decay and the observed one. These are well-known features, much discussed in the literature [42, 58, 74], but without a clear conclusion. <sup>10</sup> Our interpretation is that the observed deviation from the theoretical angular distribution can be reasonably attributed to the particular data set.

As a matter of fact, from the last two columns of table 5 we see that, when the events K13, K14, K15 and K16 are included (rather than excluded *a priori* from the analysis), the GOF of the angular distribution of Kamiokande-II improves.

Finally, let us discuss the GOF of the entire data set:

---

<sup>10</sup>There have been attempts to explain the discrepancy of the angular distribution assuming that some events are due to elastic scattering (ES) rather than inverse beta decay. For a discussion of the best candidate ES, the first Kamiokande-II event, see [58, 59]. It is not very likely that ES events are present in the data of IMB, since we expect (due to the neutrino in the final state) the visible energy to be small, and especially since none of them is well aligned with the supernova.

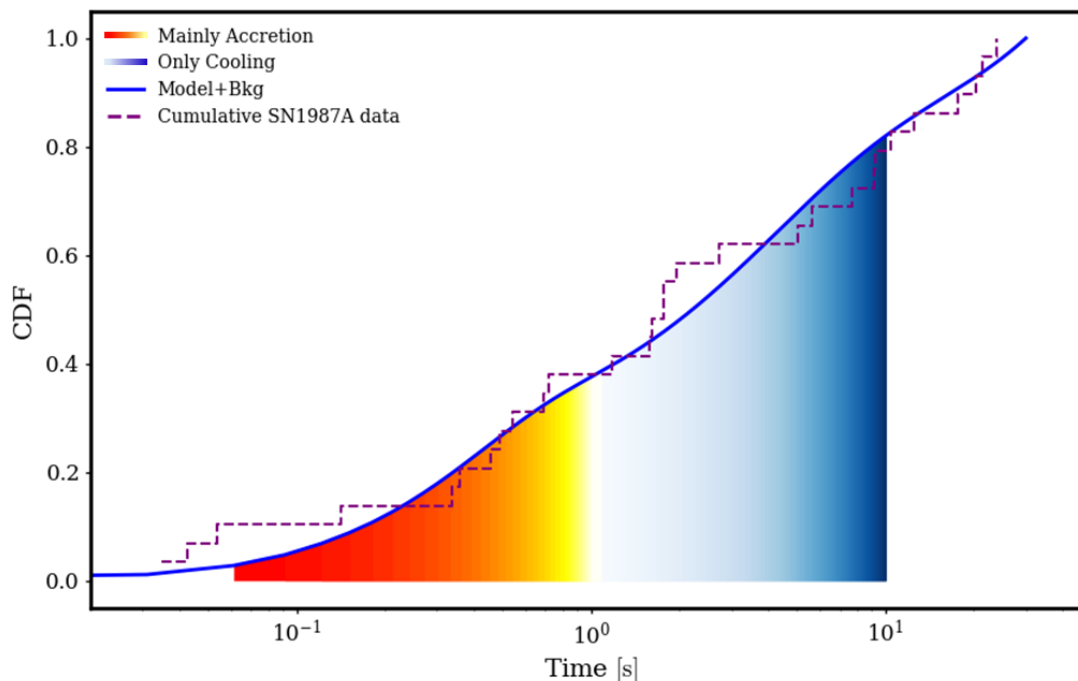


**Figure 8:** Comparison between the temporal CDF of our model and the ECDF from the data of all three experiments, including delays. The color scale is the same of figure 1, and again it helps to discriminate the two emission phases. Note the use of the logarithmic time scale.

1. energy distribution: we find a significantly better agreement with the energy CDF, as quantified by the Kolmogorov-Smirnov p-value 50.7% and Cramér-von Mises p-value 77.7%;
2. time distribution: employing the additional information on the delay times obtained from our analysis, we are able to compare the temporal CDF, which includes all three experiments, with the data. The result is displayed in figure 8. The excellent agreement is confirmed by the goodness-of-fit tests we have already used for each experiment: the Kolmogorov-Smirnov p-value is 82.8%, while the Cramér-von Mises p-value is 88.4%;
3. angle distribution: the CDF has a poorer agreement with the available empirical distributions. The Kolmogorov-Smirnov p-value is 5.5%, while the Cramér-von Mises p-value is 2.0%, which is less problematic than previous findings in literature [42, 58, 74] although not entirely satisfactory.

## 6 Conclusions

We have described the neutrino emission from SN1987, by considering the time, energy, and scattering angle of the events. We have performed a refined analysis of the data adopting a parameterized model [30]. Parametric models, characterized by physically motivated parameters, are straightforward to understand and flexible enough to accommodate future observations. Our model improves on the previous ones in literature by including an initial *finite* rise time, not yet observed because of the limited number of events but in line with the expectations. It accounts for a smooth evolution between the accretion and cooling phases of luminosity, i.e., it provides a continuous and regular curve, similar to those indicated by the simulations. We have assumed that all detected neutrino events come from inverse beta decay, which is the most relevant channel for non-thermal processes. For the IBD cross section we have adopted the most recent and accurate calculation to date [60].

In our analysis, we have exploited the energy, time and direction of arrival of the events as provided by Kamiokande-II [21, 22], IMB [23, 24] and Baksan [25]. Furthermore, we did not classify the individual events as signal or background *a priori* but analyzed them keeping into account all available information.<sup>11</sup> Throughout the analysis, we have used the information on the expected background in the experiments, considering their specific features and biases. We have recovered the intrinsic (or hardware) efficiency of each experiment as a function of energy by the best available information and reasonable extrapolation. The total efficiencies (provided by the experiments) define the total expected number of events, while the intrinsic efficiencies  $\eta$  and the resolution functions  $\sigma$  are needed to model the triple differential emission spectra.

We have performed a statistical analysis which is in several respects more refined and precise than earlier efforts in literature. The result are the best fit values of 9 parameters, describing astrophysics and detector response, together with their confidence regions. Let us underline the main results:

- we have obtained the first accurate estimates of the initial rising time  $t_{\max}$ , and of the experimental delay times. We have showed that data do not indicate a preferred value for  $t_{\max}$ , that we have set as a prior at  $t_{\max} = 100\text{ms}$ . The delay times can be calculated within uncertainties of 100 ms.
- We give accurate values for the duration of the accretion and cooling phases, in agreement with current literature. We find that the statistical significance of considering both the two primary phases, with respect to only considering the cooling phase, is 98.8-99.8%.
- The best fit values of the remaining parameters are also in accordance with current simulations of SN explosion.

---

<sup>11</sup>Indeed, in the absence of the identification of the neutron, associated to the positron in the IBD reaction, no single event can be attributed with absolute certainty to the supernova, and useful statements refer to sufficiently large subsets of data, ideally the entire data set.

- A particularly intriguing result regards the value of the fraction of neutrons involved in the emission, which for the first time align closely with expectations. Despite its large uncertainty, the value  $\xi_{n0} = 1.8\%$  suggests that during accretion,  $\bar{\nu}_e$  are produced by a neutron atmosphere around the nascent proto-neutron star thinner than expected from previous analyses [26, 27].
- Other interesting results pertain to the number of events expected as signal, together with their uncertainties, and the time windows to cumulate the 95% of the events, that we have compared with the expectations.

We have cross-checked all analyses by always using two different programming languages, Python and Mathematica. We have assessed the suitability of our model at the best fit values through goodness-of-fit tests, performed on the temporal, energy and angular distributions. We have used the Cramér–von Mises and Kolmogorov-Smirnov tests, and compared the empirical cumulative distribution function of a sample with the cumulative distribution function of a specified theoretical distribution (see figure 8). We find the description of the flux quite reliable, particularly the temporal distribution.

## 7 Acknowledgments

V.d.R. would like to thank the Quantum Theory Center (QTC) at the Danish Institute for Advanced Study and IMADA of the University of Southern Denmark for the hospitality during the completion of this work. G.R. acknowledges the support of the research projects ENP (Exploring New Physics), funded by INFN (Istituto Nazionale di Fisica Nucleare). The work of F.V. is partially supported by the grant 2022E2J4RK *PANTHEON: Perspectives in Astroparticle and Neutrino THEory with Old and New messengers*, PRIN 2022, funded by the Italian Ministero dell’Università e Ricerca (MUR) & European Union – Next Generation EU.

## References

- [1] S.A. Colgate and R.H. White, *The hydrodynamic behavior of supernovae explosions*, *Astrophysical Journal* **143** (1966) 626.
- [2] J.R. Wilson, *A numerical study of gravitational stellar collapse*, *Astrophys. J.* **163** (1971) 209.
- [3] D.K. Nadyozhin, *The neutrino radiation for the hot neutron star formation and the envelope outburst problem*, *Astrophys. Space Sci.* **53** (1978) 131.
- [4] H.A. Bethe and J.R. Wilson, *Revival of a stalled supernova shock by neutrino heating*, *Astrophys. J.* **295** (1985) 14.
- [5] A. Burrows, *Supernova neutrinos*, *Astrophysical Journal* **334** (1988) 891.
- [6] H.A. Bethe, *Supernovae*, *Physics Today* **43** (1990) 24.
- [7] S. Woosley and T. Janka, *The physics of core-collapse supernovae*, *Nature Physics* **1** (2005) 147.
- [8] H.T. Janka, K. Langanke, A. Marek, G. Martínez-Pinedo and B. Müller, *Theory of core-collapse supernovae*, *Physics Reports* **442** (2007) 38 [[astro-ph/0612072](#)].
- [9] G. Raffelt, *Neutrinos and the stars*, in *International School of Physics “Enrico Fermi”, 182nd Course, “Neutrino Physics and Astrophysics”*, vol. 182, (Villa Monastero, Varenna, Italy), pp. 61–143, arXiv, May, 2012, [DOI](#).
- [10] H.-T. Janka, *Explosion mechanisms of core-collapse supernovae*, *Ann. Rev. Nucl. Part. Sci.* **62** (2012) 407 [[1206.2503](#)].
- [11] A. Burrows, *Colloquium: Perspectives on core-collapse supernova theory*, *Rev. Mod. Phys.* **85** (2013) 245.
- [12] T. Foglizzo, R. Kazeroni, J. Guilet, F. Masset, M. González, B.K. Krueger et al., *The explosion mechanism of core-collapse supernovae: Progress in supernova theory and experiments*, *Publications of the Astronomical Society of Australia* **32** (2015) .
- [13] A. Mirizzi, I. Tamborra, H.-T. Janka, N. Saviano, K. Scholberg, R. Bollig et al., *Supernova neutrinos: Production, oscillations and detection*, *Riv. Nuovo Cim.* **39** (2016) 1 [[1508.00785](#)].
- [14] S. Horiuchi and J.P. Kneller, *What can be learned from a future supernova neutrino detection?*, *Journal of Physics G: Nuclear and Particle Physics* **45** (2018) 043002.
- [15] H.-T. Janka, *Neutrino-driven explosions*, in *Handbook of Supernovae*, pp. 1095–1150, Springer International Publishing (2017), [DOI](#).
- [16] H.-T. Janka, *Neutrino emission from supernovae*, in *Handbook of Supernovae*, A.W. Alsabti and P. Murdin, eds., (Cham), pp. 1575–1604, Springer International Publishing (2017), [DOI](#).
- [17] B. Müller, *Neutrino emission as diagnostics of core-collapse supernovae*, *Annual Review of Nuclear and Particle Science* **69** (2019) 253.
- [18] A. Mezzacappa, E. Endeve, O.E. Bronson Messer and S.W. Bruenn, *Physical, numerical, and computational challenges of modeling neutrino transport in core-collapse supernovae*, *Liv. Rev. Comput. Astrophys.* **6** (2020) 4 [[2010.09013](#)].
- [19] A. Burrows and D. Vartanyan, *Core-collapse supernova explosion theory*, *Nature* **589** (2021) 29 [[2009.14157](#)].

- [20] S.E. Woosley and T.A. Weaver, *The physics of supernova explosions*, *IN: Annual review of astronomy and astrophysics. Volume 24 (A87-26730 10-90). Palo Alto, CA, Annual Reviews, Inc., 1986, p. 205-253.* **24** (1986) 205.
- [21] K. Hirata, T. Kajita, M. Koshiba, M. Nakahata, Y. Oyama, N. Sato et al., *Observation of a neutrino burst from the supernova SN1987A*, *Phys. Rev. Lett.* **58** (1987) 1490.
- [22] K.S. Hirata, T. Kajita, M. Koshiba, M. Nakahata, Y. Oyama, N. Sato et al., *Observation in the Kamiokande-II detector of the neutrino burst from supernova SN1987A*, *Phys. Rev. D* **38** (1988) 448.
- [23] R.M. Bionta et al, *Observation of a neutrino burst in coincidence with supernova 1987A in the large magellanic cloud*, *Phys. Rev. Lett.* **58** (1987) 1494.
- [24] C.B. Bratton, D. Casper, A. Ciocio, R. Claus, M. Crouch, S.T. Dye et al., *Angular distribution of events from SN1987a*, *Phys. Rev. D* **37** (1988) 3361.
- [25] E. Alexeyev, L. Alexeyeva, I. Krivosheina and V. Volchenko, *Detection of the neutrino signal from SN 1987A in the LMC using the INR Baksan underground scintillation telescope*, *Physics Letters B* **205** (1988) 209.
- [26] T.J. Loredo and D.Q. Lamb, *Bayesian analysis of neutrinos observed from supernova SN-1987A*, *Phys. Rev. D* **65** (2002) 063002 [[astro-ph/0107260](#)].
- [27] G. Pagliaroli, F. Vissani, M.L. Costantini and A. Ianni, *Improved analysis of SN1987A antineutrino events*, *Astropart. Phys.* **31** (2009) 163.
- [28] L.F. Abbott, A. De Rujula and T.P. Walker, *Constraints on the neutrino mass from the supernova data: A systematic analysis*, *Nucl. Phys. B* **299** (1988) 734.
- [29] P. Dedin Neto, M.V. dos Santos, P.C. de Holanda and E. Kemp, *SN1987A neutrino burst: Limits on flavor conversion*, *Eur. Phys. J. C* **83** (2023) 459 [[2301.11407](#)].
- [30] F. Vissani and A. Gallo Rosso, *On the time distribution of supernova antineutrino flux*, *Symmetry* **13** (2021) .
- [31] N. Panagia, *Distance to SN 1987 a and the LMC*, in *Proceedings of the 190th IAU Symposium New Views of the Magellanic Clouds*, Y.-H. Chu, N. Suntzeff, J. Hesser and D. Bohlender, eds., p. 549, 1999, [DOI](#).
- [32] E. Roulet and F. Vissani, *Neutrinos in Physics and Astrophysics*, World Scientific (Oct., 2022), [10.1142/12982](#).
- [33] G. Ricciardi, *Introduction to Neutrino and Particle Physics*, UNITEXT for Physics, Springer (2024), [10.1007/978-3-031-65096-3](#).
- [34] G. Badino et al., *The 90 ton liquid scintillator detector in the mont blanc laboratory*, *Nuovo Cim. C* **7** (1984) 573.
- [35] M. Aglietta et al., *On the event observed in the Mont Blanc Underground Neutrino observatory during the occurrence of Supernova 1987a*, *EPL* **3** (1987) 1315.
- [36] M. Aglietta, G. Badino, G. Bologna, C. Castagnoli, A. Castellina, O. Saavedra et al., *Comments on the two events observed in neutrino detectors during the supernova 1987a outburst.*, *EPL* **3** (1987) 1321.
- [37] V.L. Dadykin et al., *Detection of a Rare Event on 23 February 1987 by the Neutrino Radiation Detector Under Mont Blanc*, *JETP Lett.* **45** (1987) 593.



- [38] O. Saavedra et al., *On the neutrino burst from SN 1987a detected in the Mt. Blanc LSD experiment*, *Nucl. Phys. B Proc. Suppl.* **3** (1988) 453.
- [39] G. Pagliaroli, F. Vissani, E. Coccia and W. Fulgione, *Neutrinos from supernovae as a trigger for gravitational wave search*, *Phys. Rev. Lett.* **103** (2009) 031102 [[0903.1191](#)].
- [40] G. Pagliaroli, M.L. Costantini, A. Ianni and F. Vissani, *The first second of SN1987A neutrino emission*, May, 2007. arXiv:0705.4032.
- [41] F. Halzen and G.G. Raffelt, *Reconstructing the supernova bounce time with neutrinos in IceCube*, *Phys. Rev. D* **80** (2009) 087301.
- [42] M.I. Krivoruchenko, *A statistical analysis of angular distribution of neutrino events observed in Kamiokande-II and IMB detectors from supernova SN1987a*, *Z. Phys. C* **44** (1989) 633.
- [43] F. Vissani, *Comparative analysis of SN1987A antineutrino fluence*, *J. Phys. G* **42** (2015) 013001 [[1409.4710](#)].
- [44] S.P. Mikheyev and A.Y. Smirnov, *Resonant neutrino oscillations in matter*, *Prog. Part. Nucl. Phys.* **23** (1989) 41.
- [45] A.S. Dighe and A.Y. Smirnov, *Identifying the neutrino mass spectrum from the neutrino burst from a supernova*, *Phys. Rev. D* **62** (2000) 033007 [[hep-ph/9907423](#)].
- [46] J.T. Pantaleone, *Neutrino oscillations at high densities*, *Phys. Lett. B* **287** (1992) 128.
- [47] M.C. Volpe, *Neutrinos from dense environments: Flavor mechanisms, theoretical approaches, observations, and new directions*, *Rev. Mod. Phys.* **96** (2024) 025004 [[2301.11814](#)].
- [48] A.Y. Smirnov, D.N. Spergel and J.N. Bahcall, *Is large lepton mixing excluded?*, *Phys. Rev. D* **49** (1994) 1389 [[hep-ph/9305204](#)].
- [49] C. Lunardini and A.Y. Smirnov, *Neutrinos from SN1987A, earth matter effects and the LMA solution of the solar neutrino problem*, *Phys. Rev. D* **63** (2001) 073009 [[hep-ph/0009356](#)].
- [50] H. Minakata and H. Nunokawa, *Inverted hierarchy of neutrino masses disfavored by supernova 1987A*, *Phys. Lett. B* **504** (2001) 301 [[hep-ph/0010240](#)].
- [51] M. Kachelriess, A. Strumia, R. Tomas and J.W.F. Valle, *SN1987A and the status of oscillation solutions to the solar neutrino problem*, *Phys. Rev. D* **65** (2002) 073016 [[hep-ph/0108100](#)].
- [52] V. Barger, D. Marfatia and B.P. Wood, *Supernova 1987A did not test the neutrino mass hierarchy*, *Phys. Lett. B* **532** (2002) 19 [[hep-ph/0202158](#)].
- [53] P.F. de Salas, D.V. Forero, S. Gariazzo, P. Martínez-Miravé, O. Mena, C.A. Ternes et al., *2020 Global reassessment of the neutrino oscillation picture*, *JHEP* **02** (2021) 071 [[2006.11237](#)].
- [54] F. Capozzi, E. Di Valentino, E. Lisi, A. Marrone, A. Melchiorri and A. Palazzo, *Unfinished fabric of the three neutrino paradigm*, *Phys. Rev. D* **104** (2021) 083031 [[2107.00532](#)].
- [55] M.C. Gonzalez-Garcia, M. Maltoni and T. Schwetz, *NuFIT: Three-flavour global analyses of neutrino oscillation experiments*, *Universe* **7** (2021) 459 [[2111.03086](#)].
- [56] W.C. Haxton, *Nuclear response of water Cherenkov detectors to supernova and solar neutrinos*, *Phys. Rev. D* **36** (1987) 2283.
- [57] R. Tomas, D. Semikoz, G.G. Raffelt, M. Kachelriess and A.S. Dighe, *Supernova pointing with*

- low-energy and high-energy neutrino detectors, *Phys. Rev. D* **68** (2003) 093013 [[hep-ph/0307050](#)].
- [58] M.L. Costantini, A. Ianni and F. Vissani, *SN1987A and the properties of neutrino burst*, *Phys. Rev. D* **70** (2004) 043006 [[astro-ph/0403436](#)].
- [59] F. Vissani and G. Pagliaroli, *Features of Kamiokande-II, IMB and Baksan observations and their interpretation in a two-component model for the signal*, *Astron. Lett.* **35** (2009) 1 [[0810.0456](#)].
- [60] G. Ricciardi, N. Vignaroli and F. Vissani, *An accurate evaluation of electron (anti-)neutrino scattering on nucleons*, *JHEP* **08** (2022) 212 [[2206.05567](#)].
- [61] D.W. Casper, L.R. Sulak, R. Bionta, G. Blewitt, C. Bratton, D. Casper et al., *Neutrino astrophysics with imb: past, present, and future*, *Nuclear Physics B - Proceedings Supplements* **3** (1988) 463.
- [62] B. Jegerlehner, F. Neubig and G. Raffelt, *Neutrino oscillations and the supernova SN1987A signal*, *Phys. Rev. D* **54** (1996) 1194 [[astro-ph/9601111](#)].
- [63] C.B. Bratton, D. Casper, A. Ciocio, R. Claus, M. Crouch, S.T. Dye et al., *Angular distribution of events from SN1987A*, *Phys. Rev. D* **37** (1988) 3361.
- [64] V. di Risi, R.M. Bozza, G. Matteucci, G. Ricciardi, V. Oliviero and F. Vissani, *An improved description of neutrino emission from SN1987a*, in *Poster for EPIC 2024 – Electroweak Physics Intersections*, (Geremeas, Cagliari, Italy), Zenodo, Sept., 2024, [DOI](#).
- [65] V. Oliviero, R.M. Bozza, V. di Risi, G. Matteucci, F. Vissani and G. Ricciardi, *Are there critical aspects in the time, energy and angular distributions of SN1987A?*, in *Proceeding for 13th Cosmic-Ray International Studies and Multi-Messenger Astroparticle Conference*, (Trapani, Italy), June, 2024, [DOI](#).
- [66] L. Lista, *Statistical Methods for Data Analysis in Particle Physics*, vol. 909, Springer (2016), [10.1007/978-3-319-20176-4](#).
- [67] K. Kotake, K. Sato and K. Takahashi, *Explosion mechanism, neutrino burst, and gravitational wave in core-collapse supernovae*, *Rept. Prog. Phys.* **69** (2006) 971 [[astro-ph/0509456](#)].
- [68] A. Marek and H.T. Janka, *Delayed neutrino-driven supernova explosions aided by the standing accretion-shock instability*, *Astrophys. J.* **694** (2009) 664 [[0708.3372](#)].
- [69] S. Algeri, J. Aalbers, K.D. Morà and J. Conrad, *Searching for new physics with profile likelihoods: Wilks and beyond*, *arXiv preprint* (2019) [[1911.10237](#)].
- [70] P. Shternin and D. Yakovlev, *A young cooling neutron star in the remnant of supernova 1987a*, *Astron. Lett.* **34** (2008) 675.
- [71] S. Orlando, M. Miceli, M.L. Pumo and F. Bocchino, *Supernova 1987A: A template to link supernovae to their remnants*, *Astrophys. J.* **810** (2015) 168.
- [72] C. Fransson et al., *Emission lines due to ionizing radiation from a compact object in the remnant of Supernova 1987A*, *Science* **383** (2024) 898 [[2403.04386](#)].
- [73] D.F.G. Fiorillo, M. Heinlein, H.-T. Janka, G. Raffelt, E. Vitagliano and R. Bollig, *Supernova simulations confront SN 1987A neutrinos*, *Phys. Rev. D* **108** (2023) 083040 [[2308.01403](#)].
- [74] A. Mal'gin, *Analysis of integral and averaged characteristics of the imb and kamioka signals from sn1987a*, *Nuovo Cim. C* **21** (1998) 317.